scientific reports

Check for updates

OPEN

Biofabrication of highly effective and easily regenerated CuO nanoparticles as adsorbents for Congo red and malachite green removal

Birhanu Asefa Ejeta[1], Gemechu Fikadu Aaga[1]✉, Workineh Mengesha Fereja[1,2] & Bekele Mengesha[1]

An effective and easily regenerated adsorbent is the one for which scientists are making an effort to explore. In this study, copper oxide nanoparticles (CuO NPs) were synthesized in a green manner from a leaf extract of Moringa stenopetala and used for dye adsorption. XRD, FTIR, and SEM were employed for the characterization of CuO NPs. The crystallite size of the CuO NPs was calculated via Debye–Scherrer equation from the XRD data and was found to be 8.33 nm. The Cu–O bonding bending vibration at 1116 cm^{-1} and stretching vibration at 1649 cm^{-1} observed from the FTIR data strongly confirmed the formation of CuO NPs. SEM morphology analysis confirmed the formation of nanoparticles with a plate-like morphology and a spherically random orientation. The zero-point charge of CuO NPs was investigated and reported to be at pH 7. The adsorption of dyes on the greenly produced CuO NPs was studied by optimizing different adsorption parameters. The removal efficiencies of the green CuO NPs adsorbent were 99.54% at the optimum conditions (pH, 4; dye concentration, 30 mg/L; amount of adsorbent, 0.25 g; and contact time, 80 min) and 98.33% at the optimum conditions (pH, 11; dye concentration, 20 mg/L; amount of adsorbent, 0.4 g; and contact time, 80 min) for congo red and malachite green, respectively. The adsorption efficiency of the biosynthesized CuO NPs for the mixture of the two dyes was 92.3%. The green synthesized adsorbent was regenerated and able to work effectively for four cycles for the two dyes. The results of the kinetics-type investigation indicate that the adsorption of both dyes by the CuO NPs adsorbent best fits a pseudo-second-order model. The isotherm model-type investigation resulted in the fitting of the Langmuir adsorption isotherm for both the congo red and malachite green dyes.

Keywords Copper oxide nanoparticles, Green synthesis, Malachite green, Congo red, Removal efficiency, Pseudokinetics study

The current interest in nanomaterials among researchers and industrial institutions is very high because of the unique characteristics of nanomaterials. Metal and metal oxide nanoparticles, metal- and nonmetal-doped nanomaterials, and nanocomposites have been synthesized, and their potential applications have been studied. In addition to the laboratory scale, different industries use nanomaterials for different purposes, including as adsorbents and catalysts in waste treatment plants[1,2], in the fabrication of energy storage devices, in energy production, and in the field of nanomedicine[3,4]. Among the different kinds of nanomaterials, metal oxide nanoparticles have attracted the attention of researchers because of their unique characteristics, i.e., being semiconducting materials that can be utilized for photocatalytic reactions[5–7], the simplicity of large-scale production at the laboratory scale, and their efficiency in application to different areas. CuO is a p-type semiconducting material that has unique properties, i.e., it is stable, can be prepared from inexpensive starting materials, and is environmentally friendly[8]. The synthesis and application of this material have been studied by different scholars, especially in waste treatment[8,9], sensors[10], and corrosion inhibition[11,12]. Using boireducing agents and capping agents from biological sources is believed to be the greenest route for the fabrication of these

[1]Department of Chemistry, College of Natural and Computational Science, Dilla University, Dilla, Ethiopia. [2]Energy and Environment Research Center, Dilla University, Dilla, Ethiopia. ✉email: gemechuf9@gmail.com

nanomaterials[13–16]. *Moringa stenopetala* can be considered a source of active bioreducing and capping agents. Alkaloids, flavonoids, tannins, saponins, amino acids, polyphenols, glycosides, and phenolic compounds are some of the bioactive compounds reported to be *present* in the leaves of *Moringa stenopetala*[17–19].

On the other hand, pollution of the environment by persistent organic pollutants is the current critical issue to be resolved by the scientific community. Among them, Congo red is the most widely used dye in textiles, plastics, cosmetics, and other academic institutions. Gastrointestinal problems, allergic reactions in the eyes and skin, blood clotting, drowsiness, respiratory difficulties, and carcinogenicity are the major health risks that Congo red can impose on humans[20–22]. The other highly toxic and widely used dye is malachite green. In addition to their advantages, they contain harmful compounds that can cause cancer, headaches, eye irritation, mutations, etc.,, in humans[23,24]. Several methods and techniques have been investigated and reported for the removal of these dyes. Among them, coagulation[25,26], flocculation[27–29], electron beam treatment[30,31], photocatalysis[32–34], and adsorption[20,35] are the most frequently used techniques. Most of these techniques are efficient for the elimination of dyes, but at the same time, they have some drawbacks. The formation of a high volume of sludge after treatment and the use of high energy, especially during beam treatment, are the major drawbacks. In most experiments and scientific reports, there are no regeneration data for adsorption[36], flocculation[37], or coagulation[38].

If it can be regenerated and used for several cycles and the production of contaminated sludge is reversed, adsorption is reported to be the most simple and available technique for the treatment of organic and inorganic wastes[39–41]. In the literature, different adsorbents from biological sources (bioadsorbents) and activated carbon from different sources have been prepared and investigated for their application. However, the problem that these adsorbents can generate is the large amount of sludge that is produced after adsorption[42,43]. The use of nanomaterials here as adsorbents seems promising. The surface area of nanomaterials makes them promising candidates for adsorption technology because they are effective adsorbents for the adsorption of pollutants, and a small amount of the nanomaterial can adsorb a large amount of the target pollutant and can be regenerated[44]. Hence, this work was designed to fabricate single, efficient, and easily regenerated CuO NPs using the leaf extract of *Moringa stenopetala* as a reducing, stabilizing, and capping agent for the adsorptive removal of Congo red and malachite green.

Methodology section

Reagents and chemicals

Analytical-grade chemicals and reagents were used for the study. Next, 95% copper nitrate trihydrate (LOBA CHEMIE), Congo red (SAMIR TECH-CHEM, LTD.), malachite green (Blulux, India) sodium hydroxide, 37% hydrochloric acid, and distilled water were used.

Experimental procedure for the preparation of CuO nanoparticles

Extraction of bioactive compounds from plant leaves

For the extraction of bioactive compounds, the leaves of *Moringa stenopetala* were collected from inside the Dilla University campus in Dilla, Ethiopia. For the collection of the leaves of *Moringa stenopetala*, permission was obtained from the Dilla University Energy and Environment Research Center. The collected leaves were cleaned by washing several times with distilled water and then drying at room temperature. For extraction purposes, the dried leaf was ground with a mortar and pestle, and 10 g of the powdered leaf was added to a flask and mixed with 100 mL of double-distilled water. The mixture was subsequently heated at 80 °C on a hot plate for 20 min. Finally, the boiled content was cooled to room temperature, and the extract was separated from the residue through filtration and then stored in a refrigerator at 4 °C[45]. All the procedures were conducted in accordance with local and national regulations.

Synthesis of copper(II) oxide nanoparticles

The synthesis of copper(II) oxide nanoparticles (CuO NPs) was performed by stirring 80 mL of copper(II) nitrate for 15 min and adding 10, 20, or 30 mL of the plant leaf extract to it. The three mixtures were stirred at 80 °C for four hours until a black color was observed. The resulting black material was subsequently powdered and calcined at 400 °C in a muffle furnace for two hours[8]. The purpose of varying the mL of plant extract was to optimize the ratio of plant leaf extract to metal ion precursor at ratios of 10:80, 20:80, and 30:80 with a constant concentration of the plant leaf extract.

Characterization of the green-synthesized CuO nanoparticles

The greenly prepared CuO NPs were characterized by scanning electron microscopy (SEM), Fourier transform infrared (FIIR) radiation, X-ray diffraction (XRD), and point-of-zero charge determination techniques. XRD was used to identify the crystalline phase and calculate the crystallite size. The experiment was performed with CuKα radiation with a wavelength of 1.5406 Å, a potential of 40 kV, and a current of 15 mA. The measurement was run at room temperature, with a 2θ value of 10° to 80°. The Debye–Scherrer formula shown in Eq. (1) was used to compute the crystallite size of the developed CuO NPs.

$$\mathrm{D} = \frac{k\lambda}{\beta\cos\theta} \tag{1}$$

where k is a constant, D is the crystallite size of the material, is the wavelength of the X-ray source, is the width at half-maximum, and θ is Bragg's diffraction angle. As the crystallite size affects the efficiency of the material, from the XRD data, CuO NPs with the smallest crystallites were selected and subjected to further characterization. The functional groups of the formed bonds in the CuO NPs and those present in the leaf extract

were investigated via FTIR spectroscopy (PerkinElmer). The morphology and dimensions of the synthesized CuO NPs were investigated via SEM (JEOL/EO-JCM-6000 Plus).

The CuO NPs point of zero charge was also investigated. To do that, 50 mL of a 0.05 M sodium chloride solution was added to different 125 mL flasks that contained 60 mg of CuO NPs, and the flasks were covered immediately. The initial pH of these solutions was varied from 1 to 9 using NaOH and HCl. The mixtures were shaken at 30 °C for 24 h. After 24 h, the contents were centrifuged at 3500 rpm for approximately 10 min. The pH values of the solutions with and without CuO NPs were measured and recorded as the pH_f and pH_i of the solutions, respectively. The value of pH_{pzc} was subsequently obtained by plotting a graph of pH_f-pH_i versus pH_i[46].

Assessment of the adsorption efficiency of CuO NPs

To assess the adsorption efficiency of the greenly produced CuO NPs, two dyes were selected, and batch adsorption was carried out. To assess its efficiency effectively, the effects of different operational parameters, such as the dye concentration, duration of contact of the adsorbate with the adsorbent pH, and adsorbent amount, were studied. After adsorption, the mixture was separated via the filtration technique and analyzed via a UV–Vis spectrophotometer at 497 and 616 nm for the remaining concentrations of congo red (CR) and malachite green (MG), respectively. Adsorption equilibrium was established between the adsorbed dyes on the adsorbent (qe) and the unadsorbed dyes in the solution. The maximum amount of dye adsorbed at equilibrium, q_e (mg/g), and the percentage of adsorbed dye were computed via Eqs. (2) and (3), respectively.

$$q_e = \frac{(C_o - C_e)\,\mathrm{V}}{m} \tag{2}$$

$$Percent\ of\ adsorption = \frac{C_o - C_e}{C_o} \times 100 \tag{3}$$

where V is the volume of the mixture in liters, C_o is the initial concentration of the dye, C_e is the equilibrium concentration of the dye, and m is the mass of the adsorbent in grams.

pH effect investigation

To determine the optimum pH for the removal of the target dyes, the other parameters were arbitrarily assigned, and the pH was varied from 2 to 9 for congo red and from 2 to 11 for malachite green. The pH of the medium itself (pH 4.6 for Congo red and pH 9.7 for malachite green) was considered one pH value when the pH of the medium was varied.

Investigations of the effects of initial dye concentrations

The initial concentration effect was investigated by varying it from 5 to 40 mg/L for congo red and from 5 to 50 mg/L for malachite green, whereas the other parameters remained constant.

Investigation of the amount of adsorbent effect

The effect of the amount of adsorbent on effective adsorption was studied. To do so, the adsorbent doses were varied from 0.01 g to 0.3 g with a gap of 0.05 g per 50 mL of 25 mg/L CR and 20 mg/L MG, while the other working parameters were maintained at previously established points.

Investigation of the optimal contact time

The amount of contact time required for the effective adsorption of the dyes was investigated by varying the contact duration from 10 to 100 min while maintaining the previously optimized parameters at their optimum values.

Real sample representation

In adsorption technology for wastewater treatment, applying a newly synthesized adsorbent to a real sample or, in the absence of a real sample, trying to provide one that represents a real sample is very important for real-world applications. Because we were not able to obtain real samples for this study, the two dyes considered for this experiment were separately prepared at the optimized concentrations (30 mg/L congo red and 20 mg/L malachite green) and mixed at 1:1 ratios at a final volume of 50 mL. For the effective analysis of the mixture of the dyes, the maximum wave length for the adsorption of the dyes was investigated from 350 nm to 650 nm, and 500 nm was found to be the maximum wavelength at which the adsorption of the mixture of the two dyes is maximal. The efficiency of the green synthesis of CuO NPs for the adsorption of a mixture of the two dyes was subsequently determined under optimized conditions via adsorption experiments.

Adsorption regeneration experiment

The importance and reliability of adsorption technology are tested by regenerating the adsorbent for repetitive use. The advantages of this work are investigated by washing the adsorbent with ethanol after adsorption and then using it for another cycle. Specifically, 50 mL of 30 mg/L and 20 mg/L solutions of congo red and malachite green, respectively, were brought into contact with the adsorbent (CuO NPs) under optimum conditions for 80 min. After 80 min, the adsorbent was separated from the solution through filtration and regenerated by washing with 50% (v/v) ethanol for another cycle of adsorption. The regeneration experiment was repeated four times. The dye concentration in ethanol was analyzed via a UV–Vis spectrophotometer[47]. The percentage of regeneration (%Re) was calculated via Eq. (4).

$$\%Re = \frac{VC_M}{Mq_e} * 100 \tag{4}$$

where V(L) and C_M represent the volume of the washed solution and the concentration of dyes in the washed solution, respectively; M(g) represents the mass of the adsorbent; and q_e represents the adsorbed dye amount obtained via Eq. (2).

Isotherm investigation

For a better understanding of the adsorption types, mechanisms, and possibilities of multilayer adsorption, the isotherms of the Langmuir and Freundlich models were considered and evaluated for fitting to the adsorption data. The Langmuir model is represented by Eq. (5)[48]:

$$q_e = \frac{q_{\max} b_{C_e}}{1 + bC_e} \tag{5}$$

where b is the isotherm constant, C_e is the concentration at equilibrium, and q_e is the adsorbed dye at equilibrium (mg/g). The linear form of the equation is given in Eq. (6):

$$\frac{1}{q_e} = \frac{1}{q_{\max}} + \frac{1}{C_e q_{\max} b} \tag{6}$$

q_{max} and b were calculated from the plot of $1/q_e$ versus $1/C_e$, respectively.

The relation shown in Eq. (6) can be used to determine the separation factor R_L:

$$R_L = \frac{1}{1 + bC_O} \tag{7}$$

where b is a constant from the Langmuir plot and C_o is the initial concentration of the dye (mg/L).

The type of adsorption reversibility is indicated by the R_L value, whether it is favorable ($0 < R_L < 1$), irreversible ($R_L = 0$), linear ($R_L = 1$), or unfavorable ($R_L > 1$).

The Freundlich adsorption isotherm is used to represent heterogeneous adsorption behavior and has an unequal distribution of active sites with different binding energies. This isotherm is represented by the relation shown in Eq. (8)[49].

$$q_e = K_f C_e^{\frac{1}{n}} \tag{8}$$

Equation (7) can be written in a linear form, as in Eq. (9).

$$\log q_e = \log K_f + \frac{1}{n} \log C_e \tag{9}$$

where C_e is the equilibrium concentration of dye, q_e is the amount of adsorbed dye at equilibrium (mg/g), K_f is the adsorbent capacity, and n is the intensity of the adsorption. K_f and n were computed from the slope and intercept, respectively, of the plot of log q_e versus log C_e.

Pseudo kinetics investigation

The pseudokinetics of both dyes were investigated, and an experiment was performed with optimized experimental parameters. For the investigation, the samples were taken for analysis at intervals of 20, 30, 40, 60, 80, 90, and 90 min, and the filtrates were quantified by a UV–visible spectrophotometer to quantify the remaining concentration. First- and second-order pseudo kinetics were examined for their fit to the adsorption data.

Results and discussion

Characterization of the green synthesized adsorbent

X-ray diffraction study

The crystalline characteristics and purity of the prepared CuO NPs were examined via X-ray diffraction (XRD). The XRD data revealed the crystalline structure of the prepared CuO NPs. Figure 1 shows the XRD pattern of the synthesized CuO NPs. X-ray diffraction peaks at 2θ values of 35.57°, 38.79°, 48.7°, 53.54°, 58.38°, 61.6°, 66.2°, 68.04°, 72.42°, and 75.1° were identified, and these diffraction peak positions matched the (1 1 0), (0 0 2), (1 1 1), (202), (020), (202), (113), (311), (113), (311), and (004) planes, respectively. The peaks obtained from the XRD pattern indicate the good crystalline monoclinic structure of CuO and are consistent with JCPDS numbers 048-1548. The obtained results are highly consistent with the previously reported literature[50]. The lattice constants of the CuO nanoparticles are $a = 4.6876$ Å, $b = 3.4104$ Å, and $c = 5.1138$ Å. The resulting XRD peaks show no other phase observed, which suggests that the green as-synthesized CuO NPs have high purity. Debye-Scherrer's formula was employed to calculate the crystalline size of the as-synthesized CuO NPs. The crystalline size was calculated for three different plant leaf extract-to-pre precursor ratios of 10:80, 20:80, and 30:80 mL, and the crystalline sizes at these ratios were determined to be 19.37 nm, 14.28 nm, and 8.33 nm, respectively, as shown in Table 1. The capping agent or stabilizer found in the plant extract controlled the growth of the nanomaterial

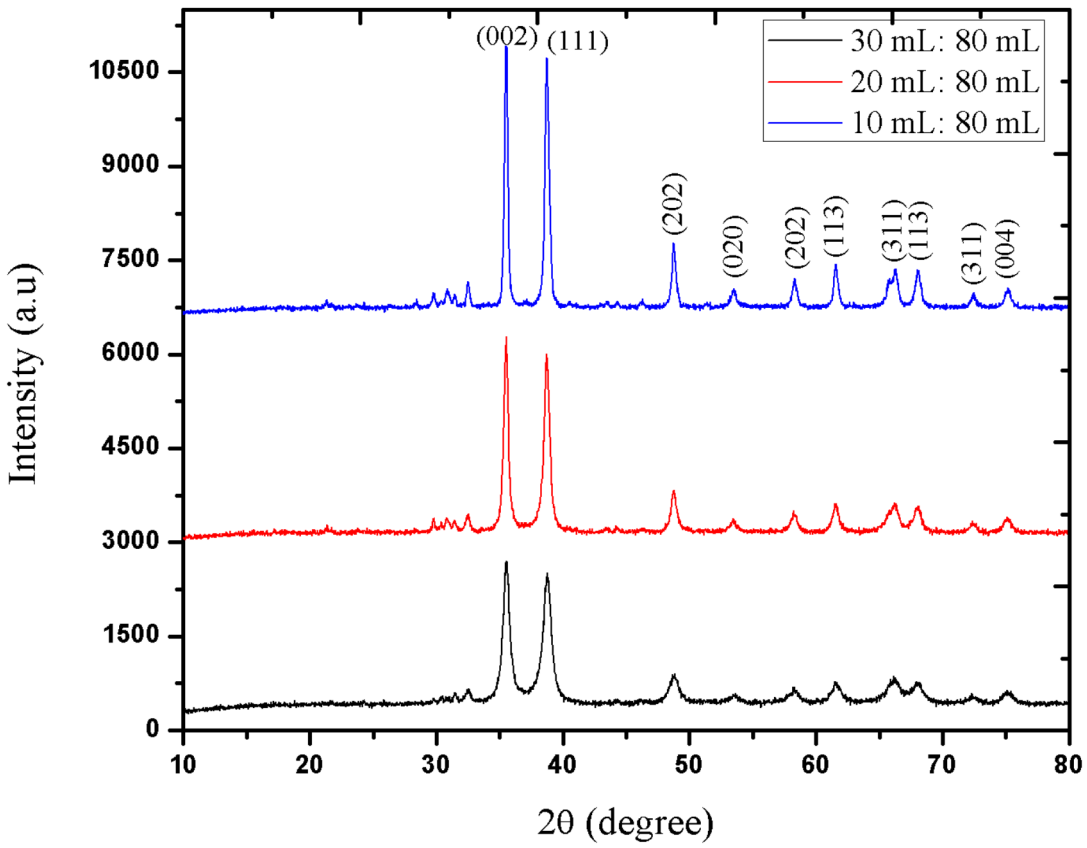

Fig. 1. XRD patterns of the synthesized copper oxide nanoparticles.

S. No	Ratio of plant extracts to precursor.	Average crystallite size.
1	NP1(30:80)	8.33
2	NP2(20:80)	14.28
3	NP3(10:80)	19.37

Table 1. CuO NPs size information for different plant extract ratios.

and prevented particle aggregation. These stabilizers are also believed to control the crystallite size of the nanoparticles; hence, at high volumes of the plant extract, a small crystallite size was obtained[51].

Fourier transform infrared study

The FTIR analysis results of the synthesized CuO NPs are shown in Fig. 2. From the FTIR spectrum of the greenly prepared CuO NPs, the adsorption peaks at 2930 and 3453 cm^{-1} correspond to the symmetric and asymmetric vibrations of the O-H bonds, respectively. These results may be due to the adsorption of moisture. On the other hand, the peaks at 1116 cm^{-1} and 1649 cm^{-1} represent the Cu-O bond bending and stretching vibrations, respectively[8]. The results of this analysis provide information about the development of the planned nanoparticles.

The phytochemicals in the leaf of the plant, which are believed to act as stabilizing and reducing agents, were also assessed via the FTIR technique. As shown in Fig. 2, the strong absorption peak observed at 3436 cm^{-1} corresponds to intermolecular oxygen-hydrogen bonds; the peak at 1644 cm^{-1} corresponds to carbonyl carbon; and the other peak at 1442 cm^{-1} corresponds to C-N stretching vibrations. These findings suggest that the oxygen-hydrogen vibration of the hydroxyl functional group at 3436 cm^{-1} and the carbon-oxygen stretching vibration of carbonyl carbon at 1644 cm^{-1} are responsible for the synthesis of CuO NPs as reducing and stabilizing agents.

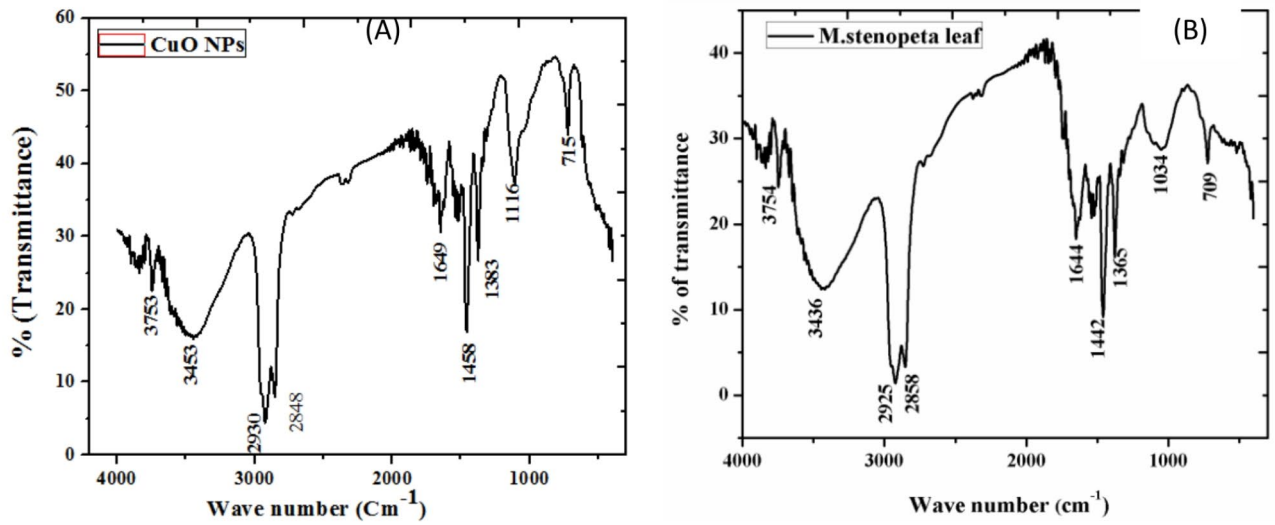

Fig. 2. Fourier transform infrared spectra of green-synthesized CuO NPs (**A**) and the leaf extract of *Moringa stenopetala* (**B**).

Surface morphology study

SEM was employed to investigate the surface morphology of the prepared CuO NPs, and the results are shown in Fig. 3. A homogeneous distribution of spherical nanoparticles with an irregular distribution was observed. SEM analysis revealed that greenly synthesized CuO NPs have a porous surface, which makes them potential adsorbents for the target pollutant. This morphology is promising for easily trapping dyes or target adsorbates[52].

Point of zero charge investigation

The point of zero charge was investigated for the green synthesized CuO NPs to determine the region of positive and negative charges on the surface of the material. The analysis results are shown in Fig. 4. The graph was drawn as ΔpH versus pH initially, and the zero point charge was considered to be the point at which the graph crossed the X axis[53], and it was found to be at pH 7. Therefore, when the solution pH is below 7, the charge on the surface of the material is positive, and when the solution pH is above 7, the surface charge is negative.

Adsorption study

Optimum pH investigation

The optimum pH for the adsorption of CR and MG dyes was investigated at pH values ranging from 2 to 9 and 2–11, respectively, and the results are shown in Fig. 5. During the investigation, other experimental parameters, such as the amount of adsorbent (0.2 g), initial concentration (30 mg/L), agitation speed (150 rpm), and duration of contact (60 min), were held constant for both dyes investigated. The adsorption efficiency for CR decreased from 99.29 to 86.11% when the pH varied from 2 to 9. For MG, the adsorption efficiency increased from 29.44 to 98.04% when the pH increased from 2 to 11. The dyes showed different adsorption behaviors with variations in pH. Minimizing the pH below the pHpzc of the CuO nanoparticles causes the surface of the nanoparticles to carry positive charges, as they can be protonated. Therefore, at this pH, anionic CR molecules can easily be adsorbed through the strong electrostatic force of attraction[54,55]. As investigated in this study, the pHpzc of the synthesized CuO NPs is 7. Therefore, when the pH of the medium is greater than 7, the surface of the nanoparticles is negatively charged, which makes the adsorption of the cationic dye MG to the surface of the CuO NPs very easy. In investigating the effect of pH, pH values of 4 and 11 were found to be the pH values at which high adsorption efficiency was obtained for the removal of CR and MG, respectively.

Investigation of the optimum initial concentration

To optimize the working parameters, the initial concentration effect was also studied by varying it from 5 to 40 mg/L for both dyes, while the other optimized working parameters were held constant. An increase in the initial concentration of the dyes resulted in a decrease in the removal efficiency of the nanoparticles for both dyes. These results are shown in Fig. 6. At 30 mg/L and 20 mg/L, the adsorption efficiency of CuO NPs was 99.14% and 96.79% for CR and MG, respectively. This trend of lower adsorption activity with increasing initial adsorbate concentration is mainly attributed to the fact that at lower adsorbate concentrations, there are more sites to adsorb the adsorbate molecules. Therefore, at this lower concentration, more adsorbate molecules are expected to be adsorbed. However, when the adsorbate amount increases, CR and MG, in our case, result in a small number of free active sites on the adsorbent surface, which is believed to decrease the removal efficiency of our adsorbent CuO NPs[56]. The result of this parameter optimization is somewhat different for these dyes, while the increasing and then decreasing removal efficiency trends are similar. The difference in removal efficiency values for the CR and MG dyes initially occurred because of the difference in the selectivity of the adsorbent

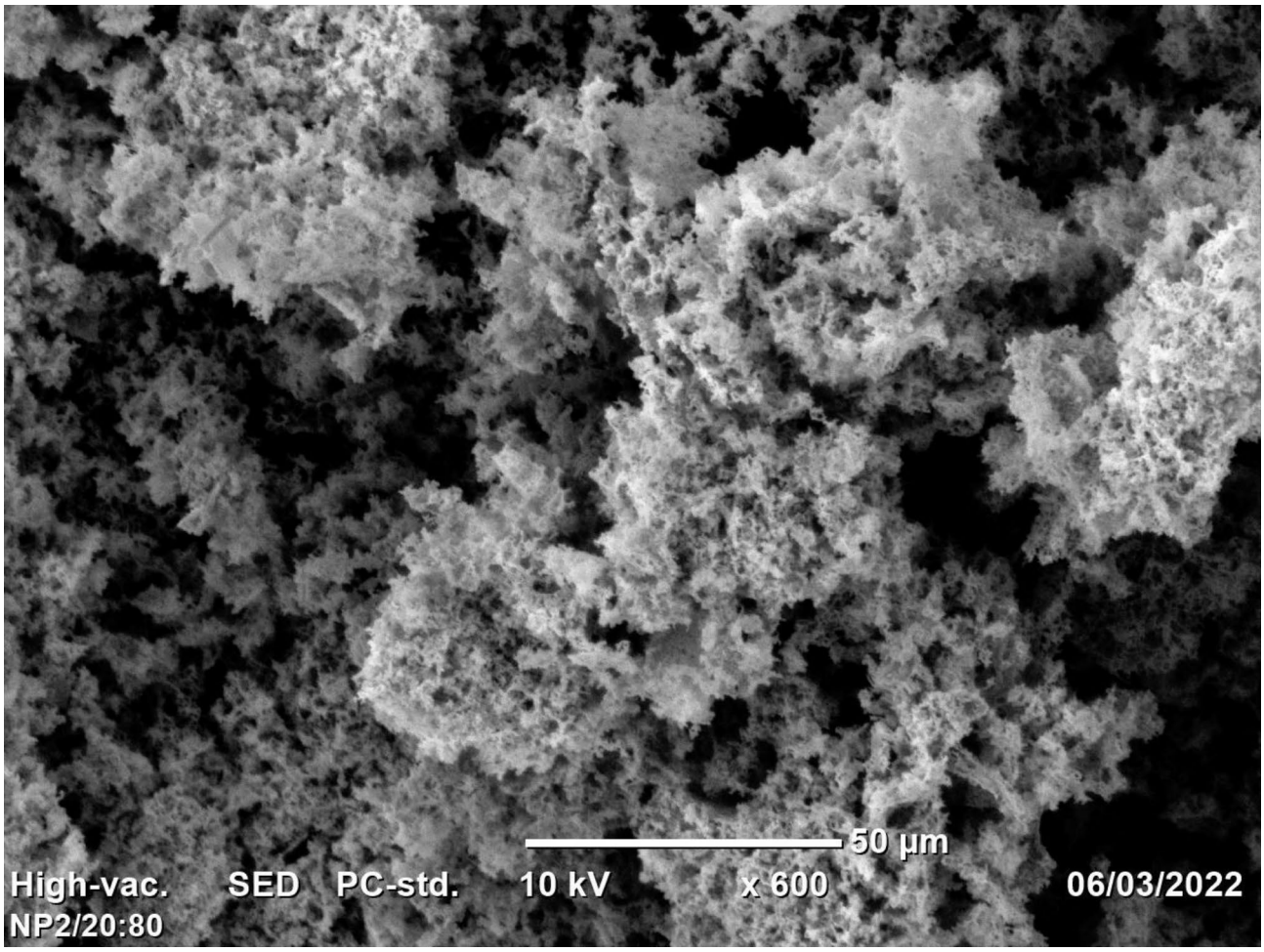

Fig. 3. Scanning electron microscope image of the synthesized CuO NPs.

toward them. The removal efficiency of the adsorbent is greater at each concentration for Congo red, which can explain the difference at the beginning of the initial concentration.

Amount of adsorbent effect

The adsorbent dose effect was also investigated as an important working parameter. For the CR dye, the amount of adsorbent varied from 0.01 g to 0.4 g. During this variation, the adsorption efficiency varied from 85.03 to 99.46% when the dose increased to 0.25 g. An increase in the adsorbent amount above 0.25 g caused the adsorption efficiency of the CR dye to decrease. An adsorbent amount of 0.25 g was considered sufficient for the effective adsorption of CR to the adsorbent surface. For the MG dye case, the adsorbent amount was varied from 0.01 g to 0.5 g by keeping the previously optimized parameters constant. In this investigation, the removal efficiency increased to 0.4 g and then decreased. As shown in Figs. 0 and 7.4 g was found to be the optimum dose, and at this dose, 97.85% removal efficiency was achieved. This trend of increasing and then decreasing adsorption efficiency can be attributed to the introduction of more active sites when the dose increased to the equilibrium point. This can be attributed to the fact that increasing the adsorbent amount up to the optimum point provides more active sites for adsorption to take place. Above the optimum point, increasing the dose may result in the overlapping of active sites and decrease the contact between adsorbate molecules and adsorbent surfaces[57]. The removal efficiency of congo red was relatively lower than that of malachite green. The molecular mass of congo red is much greater than that of malachite green. This makes Congo red very colorful even at lower concentrations. The reality resulted in a lower removal efficiency of the adsorbent at a lower dose because of the colorfulness of Congo red, which requires a greater dose amount for effective adsorption. However, when the dose increased gradually, the removal efficiency for congo red increased even more than that for malachite green because of the higher relative selectivity of the adsorbent for congo red.

Optimum time investigation

To determine the sufficient time required for complete adsorption, the duration of contact between the adsorbent and adsorbent was varied from 10 to 100 min to investigate the equilibrium time for dye adsorption. When the contact time increased from 10 to 80 min, the adsorption efficiency increased from 98.36 to 99.54% and 97.78–98.3% for CR and MG, respectively (Fig. 8). Initially, the fast increase in adsorption occurred because

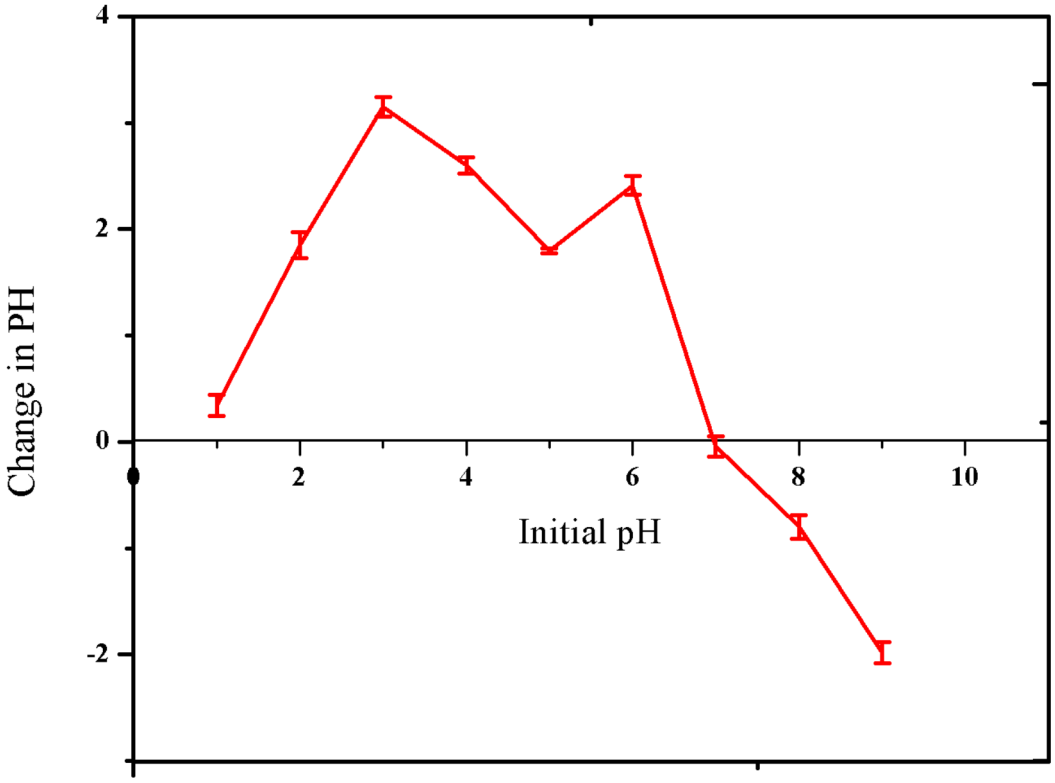

Fig. 4. Plot of the zero charge points of the synthesized CuO NPs.

of the availability of sufficient adsorption sites. However, a further increase in contact time will increase the equilibrium point, and after the equilibrium point, the surface of the adsorbent will be saturated, and further time can result in the desorption of the adsorbed dyes[58].

The results of this study under optimum conditions were also compared with those of a recent report on the adsorption of dyes with different adsorbent materials, as shown in Table 2. This study revealed that the newly prepared CuO NPs from the leaf extract of *Moringa stenopetala* had excellent adsorptive activity. Moreover, almost all the recently published reports do not include regeneration data, which is very important for adsorption to be considered a potential candidate for the removal and elimination of organic dyes from polluted environments. However, in this work, the greenly prepared CuO NPs showed excellent reusability potential, which makes them more useful for real-world applications.

Under these optimized conditions, the two dyes were mixed at 1:1 ratios and made into 50 mL in total. To accurately calculate the amount of dye in the mixture, the maximum wave length of adsorption for the mixture was determined, and the results are shown in Fig. 9. At the maximum wavelength of adsorption (500 nm), the absorbance of the mixture of dyes before and after adsorption was measured and used for the calculation of the adsorption efficiency. From the results of the adsorption experiments, the efficiency of the adsorbent for the mixture of dyes was calculated and reported to be 92.3%."

Adsorbent regeneration experiment

The results of the adsorbent regeneration study clearly indicate that the greenly synthesized CuO NPs as effective adsorbents can be regenerated and used for several cycles. The regeneration experiment for both dyes is shown in Fig. 10. These data indicate that the adsorbent was easily regenerated four times and was still working effectively. The decrease in regeneration can be due to the loss of adsorbent during washing and other active site blockage issues during multiple uses.

Adsorption isotherm investigation

The best way to explore the adsorption mechanism and solute–solution interaction is to investigate the adsorption isotherm. Two representative isotherm models (Langmuir and Freundlich) were investigated under optimum

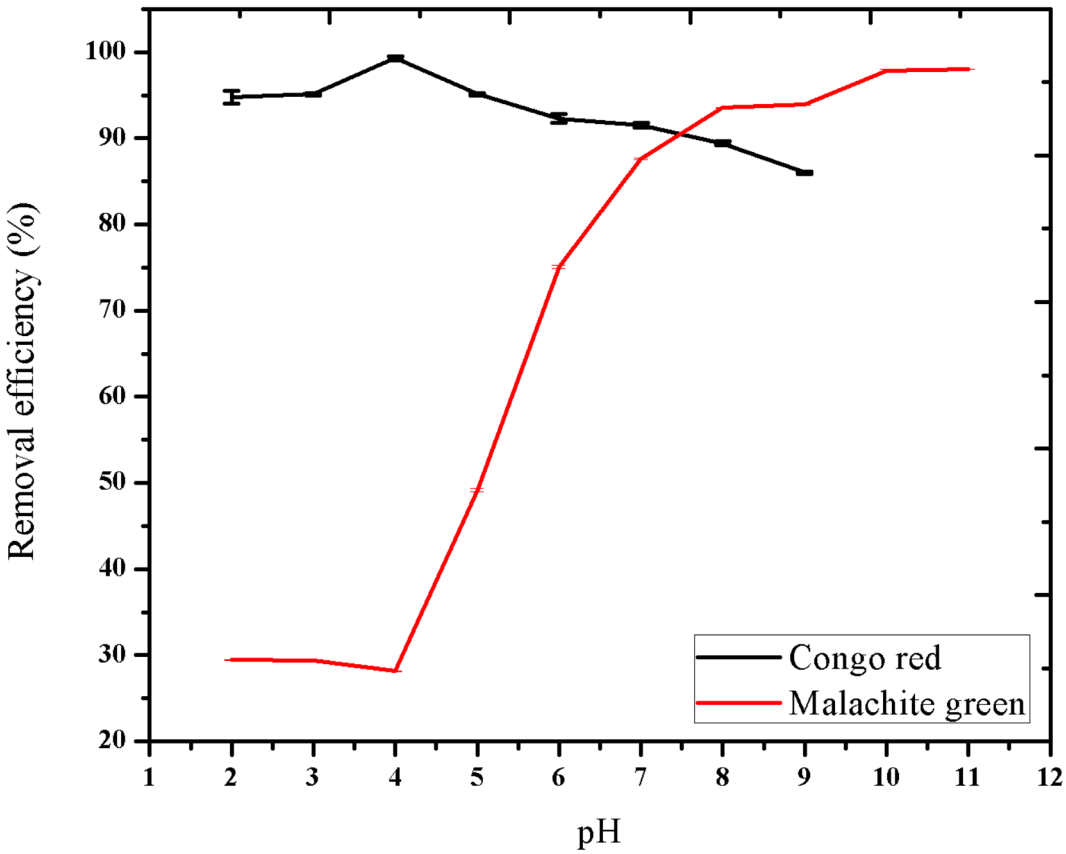

Fig. 5. Effects of pH on the adsorption of congo red and malachite green.

working parameters for this study to explain the adsorption mechanism. From the results shown in Figs. 11 and 12 and accumulated in Table 3, it is clear that the calculated data agree well with the Langmuir adsorption isotherms for both adsorbents. In this regard, the assumptions of the Langmuir model, such as monolayer coverage of the adsorbent surface, binding energy similarity on the surface adsorbent, and equal probability of the adsorbate being adsorbed everywhere on active sites, become true for this study. From this isotherm model investigation, the single-layer coverage of the surface of the adsorbent approximates physical adsorption.

Kinetics study

Kinetics is one of the experimental parameters used to study the habitation time of the adsorbate on the adsorbent, the extent of adsorption, and the adsorption mechanism. In this investigation, two kinetics models, i.e., first- and second-order pseudokinetics, were investigated under optimum conditions to predict the adsorption mechanism. For this kinetic investigation, the adsorption time was varied from 20 to 100 min while keeping the previously optimized experimental parameters constant. The integrated and linear forms of the first- and second-order kinetics models are represented by Eqs. (10) and (11), respectively.

$$\log\left(q_e - q_t\right) = logq_e - \frac{k1}{2.303} \tag{10}$$

$$\frac{1}{q_t} = \frac{1}{k_2 q_{e_2}} + \frac{1}{qe}\,\mathrm{t} \tag{11}$$

where q_e and q_t are the adsorbent's capacity (mg/g) at equilibrium and time t, respectively, and k_1 and k_2 are the first- and second-order pseudokinetics, respectively. The values of these constants were calculated from their respective graphs and are shown in Table 4. Figure 13A and B show pseudo-first-order and second-order plots of dye adsorption on CuO NPs. This experimental investigation clearly indicates that the adsorption data of both dyes best fit pseudo-second-order kinetics.

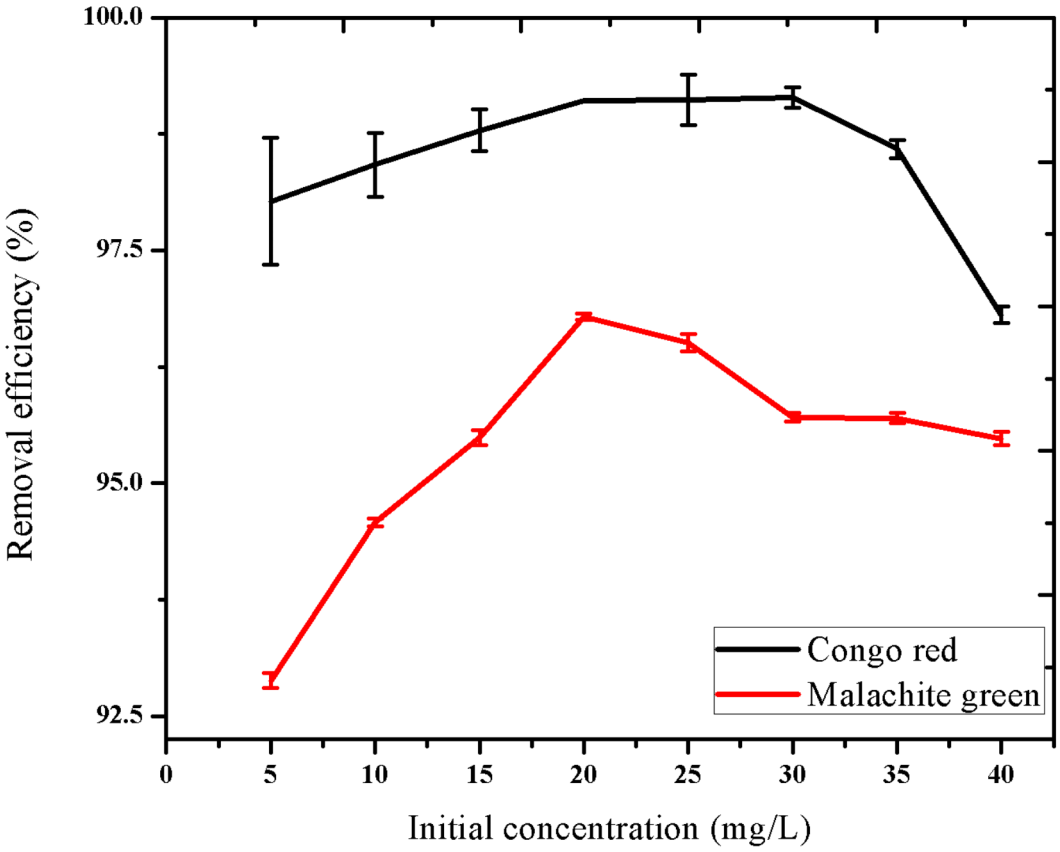

Fig. 6. Effects of initial dye concentration on the adsorption of congo red and malachite green.

Conclusion

In this study, CuO NPs were successfully synthesized via a green synthesis approach. Prior to the application of the synthesized nanoparticles, different advanced analytical techniques, such as X-ray diffraction (XRD), Fourier transform infrared (FT-IR), and scanning electron microscopy (SEM), and a pH of zero point charge were used to characterize them. The XRD characterization confirmed that the crystalline nature and crystallite size were 8.33 nm. From the FT-IR data, the characteristics of Cu–O bond formation were confirmed. In addition, the phytochemicals found in the leaves of *Moringa stenopetala* were explored. The zero-point charge pH of the prepared CuO NPs was determined and reported to be 7. Batch adsorption experiments performed on the two dyes strongly confirmed that the green-synthesized CuO NPs were the best adsorbents. The results of this study confirmed that the efficiency of adsorption of the adsorbent is strongly dependent on different adsorption parameters, such as the duration of contact, amount of adsorbent, pH of the medium, and initial dye concentration. Under optimum conditions (adsorbent dose of 0.25 g, initial adsorbate concentration of 30 mg/L, contact time of 80 min, and pH of 4), the removal efficiency was 99.54% for CR. A 98.85% removal efficiency was also obtained for MG at the optimum adsorption parameters (adsorbent dose of 0.4 g, initial adsorbate concentration of 20 mg/L, contact time of 80 min, and pH of 11). In addition, the adsorbent showed 92.3% adsorption efficiency for the mixture of dyes. A four-cycle adsorbent regeneration study revealed that the greenly developed adsorbent can be recycled and used several times. Generally, CuO NPs can be considered adsorbents for dye adsorption when a small quantity of the adsorbent is used.

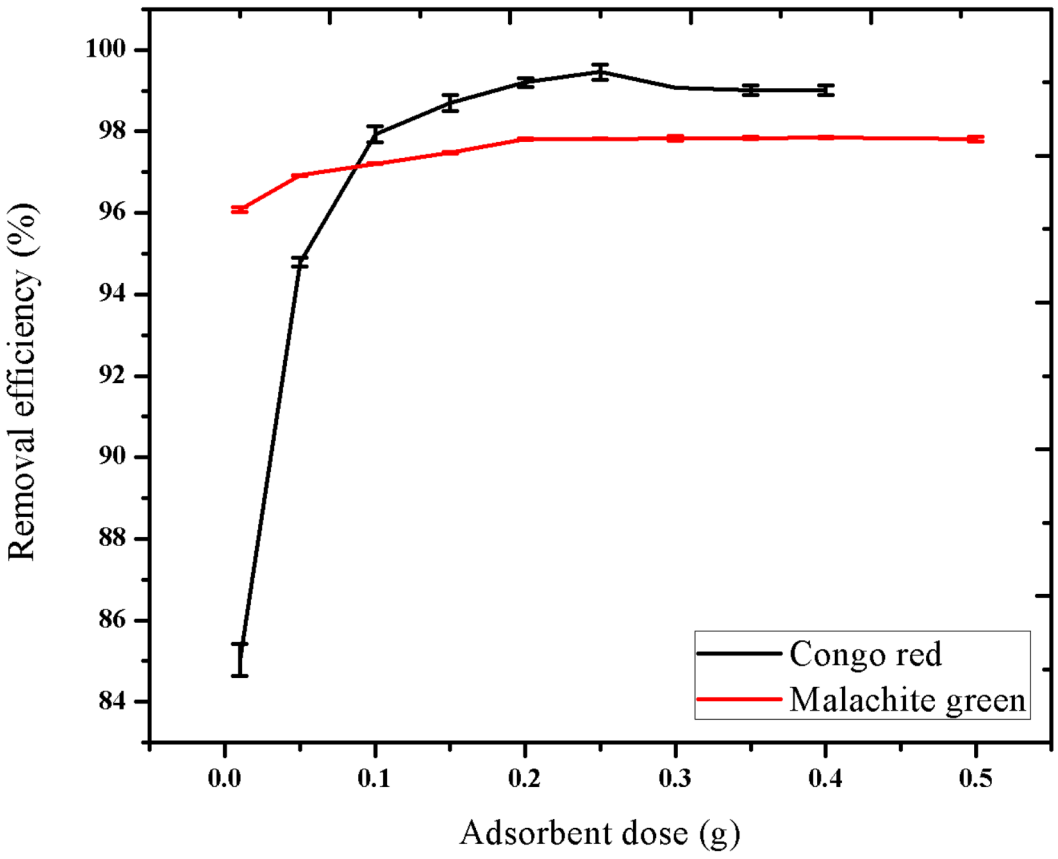

Fig. 7. Adsorbent amount effect on the removal of Congo red and malachite green.

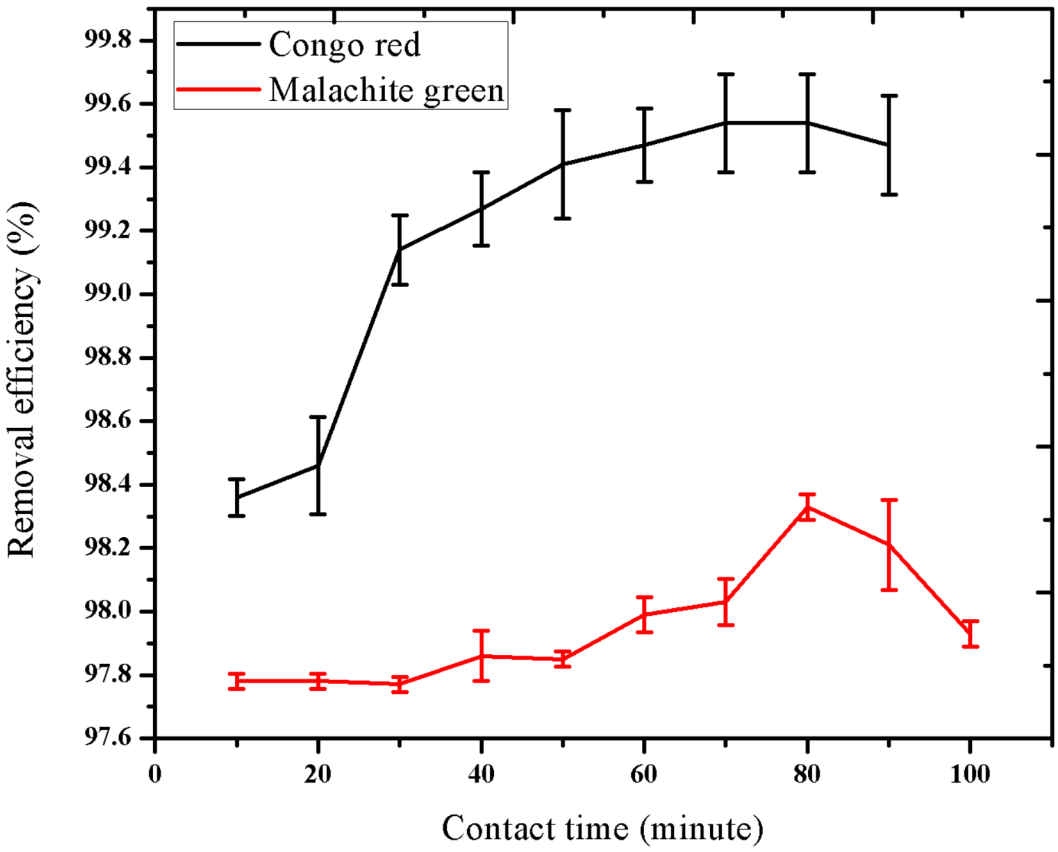

Fig. 8. Contact time effect on the removal of congo red and malachite green.

Material	Targeted pollutant	Reaction condition	Removal efficiency	Regeneration	Reference
Luffa modified with silver nanoparticles (LF/AgNPs)	Ketoprofen and reactive yellow 15	pH, 5 and 2, contact time 60 and 40 min, initial concentration 100 and 25 mg/L, respectively and adsorbent dose 25 mg	97 and 99%, respectively	No	35
Plant-derived amyloid fibril	Eosin Y and congo red	Contact time, 120 min, and 30 min, respectively	60% and 80%, respectively	No	21
Iron oxide-commercial activated carbon nanocomposite	Mordant violet 40	pH, 2.07, initial concentration, 100 mg/L, dose 100 mg, contact time, 3 h	99.92%	No	59
Amino-ethyl chitosan hydrogel	Methyl orange	pH, 7, initial concentration 25 mg/L, dose 100 mg, contact time, 60 min	100%	Yes	60
CuO NPs synthesized by flame pyrolysis	Congo red	Initial concentration 17 mg/L,	99.9%	No	61
CuO NPs synthesized by leaf extract of *Eucalyptus Globoulus*	Methyl orange	pH, 6, initial concentration, 45 mg/L, dose 45 mg	92.2 mg/g	No	62
CuO NPs synthesized by leaf extract of *Moringa stenopatalla*	Congo red and malachite green	pH, 4 and 11, initial concentration, 30 and 20 mg/L, dose 0.25 and 0.4 g, respectively and contact time, 80 min.	99.54 and 98.33%, respectively	Yes	This work

Table 2. Comparison of the adsorption efficiency and adsorbent regeneration of newly prepared CuO NPs with those reported in the literature.

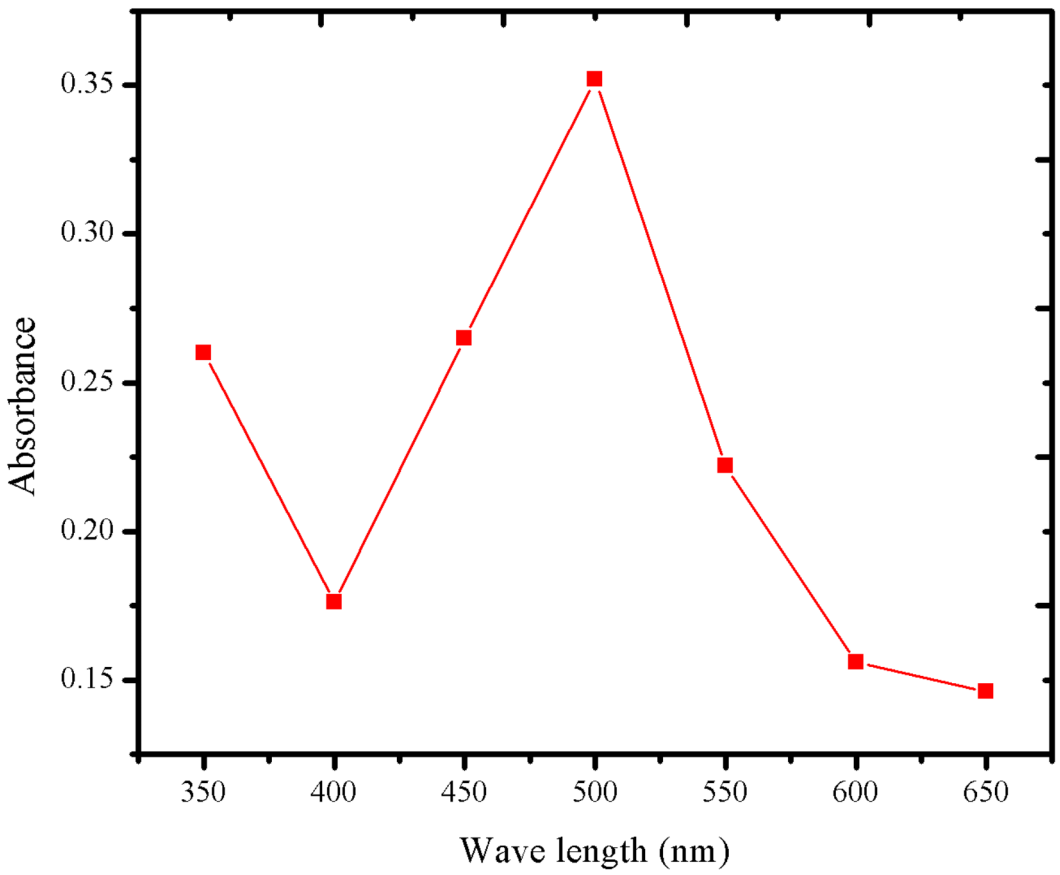

Fig. 9. Maximum wavelength of adsorption for the mixture of congo red and malachite green.

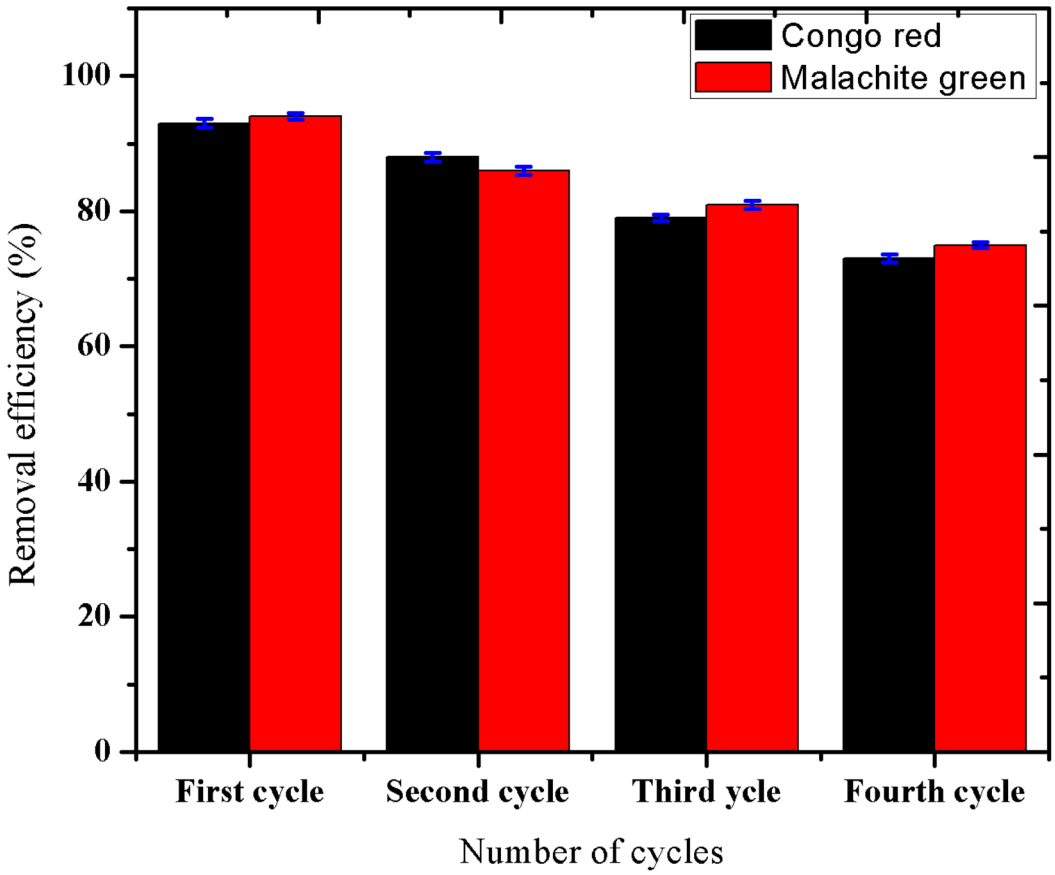

Fig. 10. Regeneration cycles.

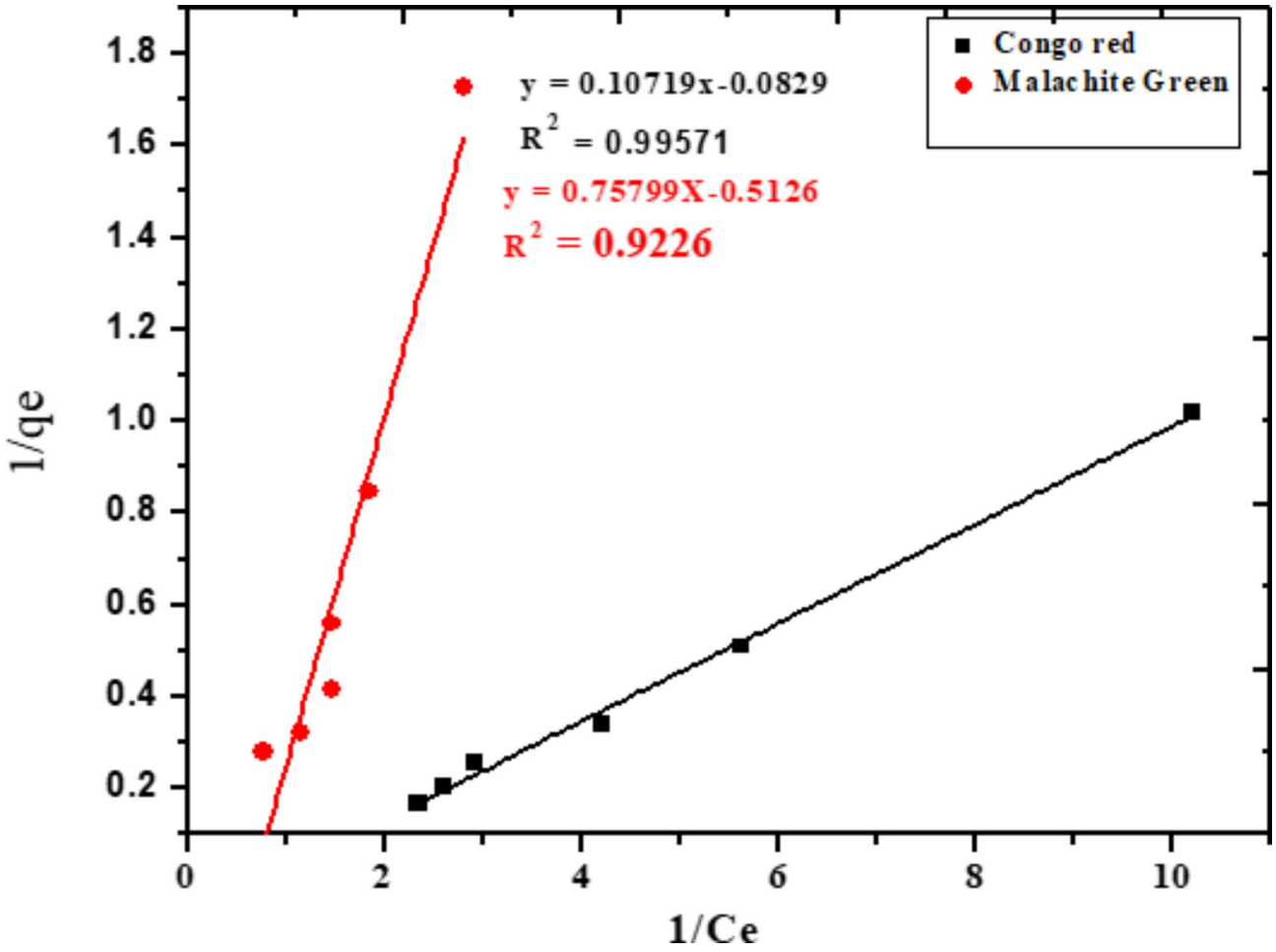

Fig. 11. Langmuir adsorption isotherm plot.

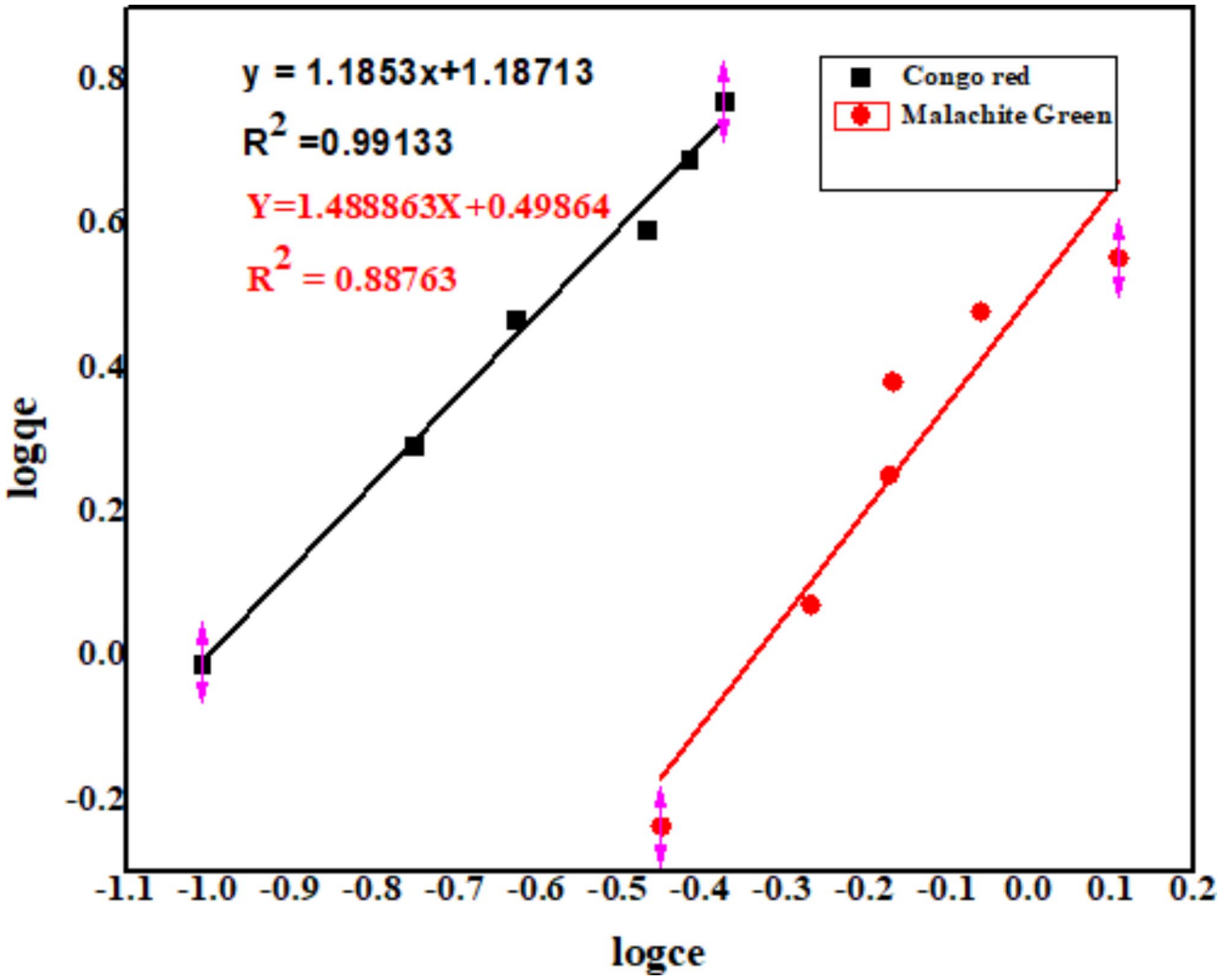

Fig. 12. Freundlich adsorption isotherm plot.

Dyes	Constants of Langmuir model				Constants of Freundlich model		
	q_{max}(mg/g)	R_L	b(L/mg)	R^2	K_f(1/mg)	N	R^2
Congo red	12.0627	0.041324	0.7733	0.99571	1.1853	0.84236	0.99133
Malachite Green	1.95083	0.05353	0.8839	0.9226	1.488863	2.0054	0.88763

Table 3. Summary of the calculated constants for the Langmuir and Freundlich isotherms.

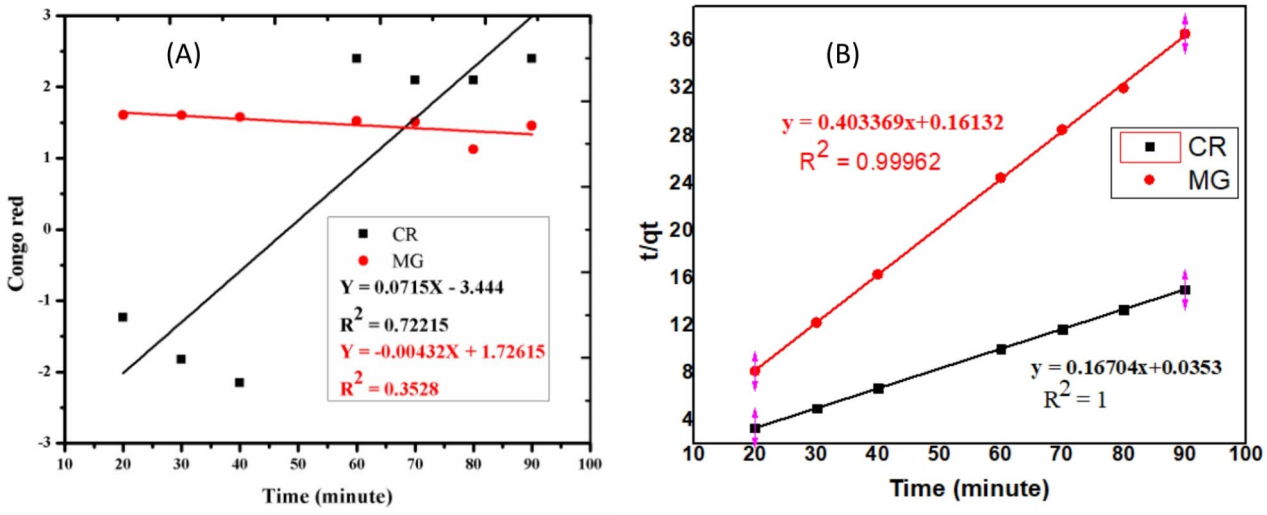

Fig. 13. Graph of the pseudo-first-order (**A**) and pseudo-second-order (**B**) kinetic models.

Model types	Selected dyes	Calculated constant parameters			
		$q_{e,exp}$.(mg/g)	$q_{e,cal}$.(mg/g)	K	R^2
Pseudo-first order	Congo red	5.964	0.031908	0.01917	0.72215
	Malachite Green	2.4200	5.618979	0.000054	0.3528
Pseudo-Second order	Congo red	5.964	5.986	0.8084	1
	Malachite Green	2.4200	2.4778	0.9126	0.99962

Table 4. Correlation coefficients and constant parameters calculated for the kinetic models.

Data availability

he datasets used and/or analysed during the current study available from the corresponding author on reasonable request.

Received: 29 March 2024; Accepted: 30 September 2024
Published online: 15 October 2024

References

1. Ngasotter, S. et al. Crustacean shell waste derived chitin and chitin nanomaterials for application in agriculture, food, and health–A review. *Carbohydr. Polym. Technol. Appl.* **2023**, 100349 .
2. Sridevi, M. et al. Role of nanomaterial's as adsorbent for heterogeneous reaction in waste water treatment. *J. Mol. Struct.* **1241**, 130596 (2021).
3. Zhu, D. et al. Recent advance in tailoring the structure and functions of self-assembled peptide nanomaterials for biomedical applications. *Coord. Chem. Rev.* **494**, 215374 (2023).
4. Liu, H. et al. Nanomaterials-based photothermal therapies for antibacterial applications. *Mater. Des.*, 112231. (2023).
5. Muthukumar, P. et al. Plasmonic nanoparticles doped metal oxide hybrid materials for efficient photocatalytic dye degradation and strong anti-biofilm activity. *Mater. Sci. Eng. B.* **296**, 116688 (2023).
6. Singh, A., Gogoi, H. P. & Barman, P. Synthesis of metal oxide nanoparticles by facile thermal decomposition of new Co (II), ni (II), and zn (II) Schiff base complexes-optical properties and photocatalytic degradation of methylene blue dye. *Inorg. Chim. Acta*. **546**, 121292 (2023).
7. Aaga, G. F., Fereja, W. M., Tolcha, D. N. & Labena, A. A. Croton macrostachyus leaf extract mediated synthesis of highly efficient ZnO NPs and ZnO/bentonite nanocomposites for photocatalytic degradation of organic dyes under solar irradiation. *J. Environ. Chem. Eng.* **11**(5), 110982 (2023).
8. Aaga, G. F. & Anshebo, S. T. Green synthesis of highly efficient and stable copper oxide nanoparticles using an aqueous seed extract of Moringa stenopetala for sunlight-assisted catalytic degradation of Congo red and alizarin red s. *Heliyon* **9**(5). (2023).
9. Nayak, R. et al. Fabrication of CuO nanoparticle: An efficient catalyst utilized for sensing and degradation of phenol. *J. Mater. Res. Technol.* **9**(5), 11045–11059 (2020).
10. Solhi, M., Rahsepar, M., Asl, A. A. K. & Kim, H. Synthesis and characterization of a high-performance enzyme-free glucose sensor based on mesoporous copper oxide nanoparticles. *Mater. Res. Bull.* **164**, 112240 (2023).
11. Devadoss, D., Asirvatham, A., Kujur, A., Saaron, P. G. & Devi, J. N. Green synthesis of copper oxide nanoparticles from Murraya koenigii and its corrosion resistivity on Ti-6Al-4V dental alloy. *J. Mech. Behav. Biomed. Mater.*, 106080. (2023).
12. Bhawsar, J. et al. Green corrosion inhibition and DFT studies of phytoextract and green synthesis of copper nanoparticles of Jacaranda mimosaefolia. *Mater. Today Proc.* (2023).
13. Shanableh, A., Bhattacharjee, S. & Sadik, S. Evaluating iron-based nanoparticles for ciprofloxacin removal: Date seed extract as a biostabilizing and a bioreducing agent. *J. Water Process. Eng.* **44**, 102419 (2021).
14. Venkatesan, S. et al. Methylene blue dye degradation potential of zinc oxide nanoparticles bioreduced using Solanum trilobatum leaf extract. *Res. Chem.* **4**, 100637 (2022).
15. Li, J. et al. Green synthesis of gold nanoparticles using potato starch as a phytochemical template, green reductant and stabilizing agent and investigating its cytotoxicity, antioxidant and anti-ovarian cancer effects. *Inorg. Chem. Commun.* **155**, 111002 (2023).
16. Thakur, T. M., Lokhande, R. S., Thigle, M. M. & Patil, V. R. Nanoparticles of chromium oxide by green synthesis using Eucalyptus globulous leaves extract; Characterization and biological activity studies. *Mater. Today Proc.* **79**, 100–106. (2023).
17. Metsopkeng, C. et al. Comparative study of Moringa stenopetala root and leaf extracts against the bacteria Staphyloccocus aureus strain from aquatic environment. *Sci. Afr.* **10**, e00549 (2020).
18. Toma, A., Makonnen, E., Mekonnen, Y., Debella, A. & Addisakwattana, S. Intestinal α-glucosidase and some pancreatic enzymes inhibitory effect of hydroalcholic extract of Moringa stenopetala leaves. *BMC Complement. Altern. Med.* **14**, 1–5 (2014).
19. Yikna, B. B. & Yehualashet, A. S. Medicinal plant extracts evaluated in vitro and in vivo for antidiabetic activities in Ethiopia: Bases for future clinical trials and related investigations. *Evid.-Based Complement. Altern. Med.* 2021. (2021).
20. Abdallah, M. A. M. & Alprol, A. E. Utilization of aquatic biomass as biosorbent for sustainable production of high surface area, nano-microporous, for removing two dyes from wastewater. *Sci. Rep.* **14**(1), 4471 (2024).
21. Yang, D-D., Chang, F-X., Zhang, B-F. & Yong, Y-C. Wheat flour-derived amyloid fibrils for efficient removal of organic dyes from contaminated water. *Bioresour. Bioprocess.* **11**(1), 1–9 (2024).
22. Hamad, K. H. et al. Nylon fiber waste as a prominent adsorbent for Congo red dye removal. *Sci. Rep.* **14**(1), 1088 (2024).
23. Abu Elella, M. H. et al. Novel high-efficient adsorbent based on modified gelatin/montmorillonite nanocomposite for removal of malachite green dye. *Sci. Rep.* **14**(1), 1228 (2024).
24. Li, X. et al. Facile preparation of sodium alginate gel beads enhanced by polyamino-modified 3D carbon for efficient remediation of organic dyes in wastewater. *Sep. Purif. Technol.*, 126637. (2024).
25. Li, P., Zhang, J., Yu, Y., Jia, W. & Zhao, S. A collaborative coagulation strategy for algae-laden and dye-containing water treatment. *J. Clean. Prod.*, 141146. (2024).
26. Sebastian, S. L. et al. Electrocoagulation using Ti/Ti for the remediation and reuse of aqueous Dispersive Blue-79. *Environ. Monit. Assess.* **196**(2), 177 (2024).
27. Chang, N., Cao, S., Li, J., Zhang, H. & Wang, H. Preparation of starch-based cationic flocculants and its study on the removal of textile dyes. *Ind. Eng. Chem. Res.* (2023).
28. Song, L. et al. Preparation of a magnetic polysilicate composite flocculant for dye wastewater treatment. *Water Air Soil Pollut.* **235**(2), 101 (2024).
29. Zhang, H. et al. Preparation of crosslinking-grafting cationic starch flocculant and its study on textile dyes removal. *J. Polym. Environ.* **2024**, 1–15.
30. Elkenawy, N. M. & Gomaa, O. M. Sequential electron beam and bioflocculation for treatment of textile nanodyes. *RSC Adv.* **13**(31), 21558–21569 (2023).
31. Liu, X. & Wang, J. Decolorization and degradation of various dyes and dye-containing wastewater treatment by electron beam radiation technology: An overview. *Chemosphere*, 141255. (2024).
32. Al-Ansari, S. H., Gomaa, H., Abdel-Rahim, R. D., Ali, G. A. & Nagiub, A. M. Recycled gold-reduced graphene oxide nanocomposite for efficient adsorption and photocatalytic degradation of crystal violet. *Sci. Rep.* **14**(1), 4379 (2024).
33. Wang, Z. et al. Layered double hydroxide helps LaFeO3 photocatalyst activate peroxymonosulfate to efficiently degrade dyes. *Sep. Purif. Technol.*, 126832. (2024).
34. Masula, K., Kore, R., Bhongiri, Y., Pola, S. & Basude, M. Ag-Li-ZnO nanostructures for efficient photocatalytic degradation of Organic dyes and Textile Wastewater under visible light treatment. *J. Mol. Struct.*, 137750. (2024).
35. Tavassoli, S. et al. Optimization and characterization of silver nanoparticle-modified luffa for the adsorption of ketoprofen and reactive yellow 15 from aqueous solutions. *Sci. Rep.* **14**(1), 4398 (2024).
36. Abas, K. M. & Al Kiey, S. A. Facile synthesis of MOF-derived N doped ZnO/C nanoparticles and its adsorption activity toward dye removal. *BMC Chem.* **17**(1), 126 (2023).

37. Moghaddam, S. S., Moghaddam, M. A. & Arami, M. Coagulation/flocculation process for dye removal using sludge from water treatment plant: Optimization through response surface methodology. *J. Hazard. Mater.* **175**(1–3), 651–657 (2010).
38. Mcyotto, F. et al. Effect of dye structure on color removal efficiency by coagulation. *Chem. Eng. J.* **405**, 126674 (2021).
39. Sitab, A. A., Tujjohra, F., Rashid, T. U. & Rahman, M. M. Thermally crosslinked electrospun nanofibrous mat from chrome-tanned solid wastes for cationic dye adsorption in wastewater treatment. *Clean. Eng. Technol.* **13**, 100621 (2023).
40. Mohamed, R. M. Surface modified Acacia Senegal Gum based spherical hydrogel; Fabrication, characterization, and kinetically optimized waste water treatment with remarkable adsorption efficiency. *Heliyon* (2023).
41. Abdel-Gawwad, H. A. et al. Utilization of red clay brick waste in the green preparation of an efficient porous nanocomposite for phenol adsorption: Characterization, experiments and statistical physics treatment. *Sustain. Chem. Pharm.* **32**, 101027 (2023).
42. Zhang, X., Bhattacharya, T., Wang, C., Kumar, A. & Nidheesh, P. V. Straw-derived biochar for the removal of antibiotics from water: Adsorption and degradation mechanisms, recent advancements and challenges. *Environ. Res.* :116998. (2023).
43. Ouyang, H. et al. Agricultural waste-derived (nano) materials for water and wastewater treatment: Current challenges and future perspectives. *J. Clean. Prod.*, 138524. (2023).
44. Inamdar, A. K. et al. A review on environmental applications of metal oxide nanoparticles through waste water treatment. *Mater. Today Proc.* (2023).
45. Steinmuller, N., Sonder, K. & Kroschel, J. Fodder tree research with Moringa stenopetala: A daily leafy vegetable of Konso people. In.: Ethiopia (2002).
46. Prola, L. D. et al. Comparison of Jatropha curcas shells in natural form and treated by non-thermal plasma as biosorbents for removal of reactive red 120 textile dye from aqueous solution. *Ind. Crops Prod.* **46**, 328–340 (2013).
47. Bavi, A., Jafari, M. S., Heydari, M., Ebrahimi, F. & Sadeghizadeh, A. Batch and continuous mode adsorption of methylene blue cationic dye onto synthesized titanium dioxide/polyurethane nanocomposite modified by sodium dodecyl sulfate. *Colloids Surf. C Environ. Aspects*. **1**, 100012 (2023).
48. Robert, L., Joseph, F. & Alexander, A. Fisher's contact dermatitis in textiles and shoes. *BC Decker Inc Ont.*, 339–401. (2008).
49. Manu, B. & Chaudhari, S. Decolorization of indigo and azo dyes in semicontinuous reactors with long hydraulic retention time. *Process Biochem.* **38**(8), 1213–1221 (2003).
50. Fang, Y. et al. CuO/TiO_2 nanocrystals grown on graphene as visible-light responsive photocatalytic hybrid materials. *Bull. Mater. Sci.* **35**, 495–499 (2012).
51. Arunachalam, J. Green synthetic route for the size controlled synthesis of biocompatible gold nanoparticles using aqueous extract of garlic (Allium Sativum). *Adv. Mater. Lett.* **4**(7), 548–555 (2013).
52. Ighalo, J. O. et al. A review of pine-based adsorbents for the adsorption of dyes. *Biomass-Derived Mater. Environ. Appl.* **2022**, 319–332 .
53. Ai, L. et al. Removal of methylene blue from aqueous solution with magnetite loaded multi-wall carbon nanotube: Kinetic, isotherm and mechanism analysis. *J. Hazard. Mater.* **198**, 282–290 (2011).
54. Salleh, M. A. M., Mahmoud, D. K., Karim, W. A. W. A. & Idris, A. Cationic and anionic dye adsorption by agricultural solid wastes: A comprehensive review. *Desalination*. **280**(1–3), 1–13 (2011).
55. Dawood, S. & Sen, T. K. Removal of anionic dye Congo red from aqueous solution by raw pine and acid-treated pine cone powder as adsorbent: Equilibrium, thermodynamic, kinetics, mechanism and process design. *Water Res.* **46**(6), 1933–1946 (2012).
56. Manzar, M. S. et al. Synthesis and characterization of a series of cross-linked polyamines for removal of Erichrome Black T from aqueous solution. *Chin. J. Chem. Eng.* **32**, 341–352 (2021).
57. Kataria, N. & Garg, V. Removal of Congo red and brilliant green dyes from aqueous solution using flower shaped ZnO nanoparticles. *J. Environ. Chem. Eng.* **5**(6), 5420–5428 (2017).
58. Mutukwa, D., Taziwa, R. T. & Khotseng, L. Antibacterial and photodegradation of Organic dyes using Lamiaceae-mediated ZnO nanoparticles: A review. *Nanomaterials*. **12**(24), 4469 (2022).
59. Mohamed, S. M. I., Yılmaz, M., Güner, E. K. & El Nemr, A. Synthesis and characterization of iron oxide-commercial activated carbon nanocomposite for removal of hexavalent chromium (Cr6+) ions and mordant Violet 40 (MV40) dye. *Sci. Rep.* **14**(1), 1241 (2024).
60. Tamer, T. M. et al. Development of novel amino-ethyl chitosan hydrogel for the removal of methyl orange azo dye model. *Sci. Rep.* **14**(1), 1284 (2024).
61. Inamdar, A. K., Rajenimbalkar, R. S., Thabet, A. E., Shelke, S. B. & Inamdar, S. N. Environmental applications of flame synthesized CuO nanoparticles through removal of Congo Red dye. *Mater. Today Proc.* (2023).
62. Alhalili, Z. Green synthesis of copper oxide nanoparticles CuO NPs from Eucalyptus Globoulus leaf extract: Adsorption and design of experiments. *Arab. J. Chem.* **15**(5), 103739 (2022).

Acknowledgements

The authors fully acknowledge Dilla University for its laboratory facilities.

Author contributions

Authors B.A. and G.F. designed the work. Author B.A. performed the lab work. Author G.F. drafted and edited the manuscript. Authors W.M. and B.M. had supervision role.

Declarations

Competing interests

The authors declare no competing interests.

Additional information

Correspondence and requests for materials should be addressed to G.F.A.